



# Synthesis, characterization and catalytic applications of CuO–NiO bimetallic oxide nanoparticles towards the reduction of hazardous pollutants, derivative preparation and cross linking reaction

M. F. Parveen<sup>1</sup> · A. Amala Jeya Ranchani<sup>2</sup> · V. Parthasarathy<sup>2</sup> · R. Anbarasan<sup>3</sup>

Received: 26 October 2021 / Accepted: 19 December 2021 / Published online: 11 January 2022  
© King Abdulaziz City for Science and Technology 2022

## Abstract

The CuO–NiO bimetallic oxide nanoparticle (BMNP) was synthesized via a chemical route by varying the concentration of Ni<sup>2+</sup>. The prepared CuO–NiO BMNP was investigated using various analytical instruments. The direct bandgap of CuO–NiO BMNP was decreased from 5.45 to 4.85 eV with the increasing concentration of Ni<sup>2+</sup>. The XRD of the prepared sample confirmed the formation of a mixture of CuO–NiO BMNP. The crystallite size was calculated as 32 nm. The FT-IR spectrum showed the metal oxide stretching around 450–700 cm<sup>-1</sup>. The HR-TEM confirmed the BMNP formation with a particle size less than 20 nm. The catalytic activity of CuO–NiO BMNP was tested towards the reduction of a mixture of hazardous pollutants present in the effluent. The apparent rate constant ( $k_{app}$ ) values were determined as  $0.0217 \times 10^{-2} \text{ s}^{-1}$  for reduction of Cr(VI) and  $0.0212 \times 10^{-2} \text{ s}^{-1}$  for reduction of Flur dye, respectively. The catalytic role of CuO–NiO BMNP was further confirmed by synthesizing the derivatives of indole and brilliant green (BG) dye. The experimental results were carefully analyzed and compared with the literature report.

**Keywords** CuO–NiO BMNP · Synthesis · Characterization · HR-TEM · Indole derivative

## Introduction

Recently, the bimetallic oxide nanoparticle (BMNP)-based nanocatalysts are very much useful in the catalysis field due to their high activity towards the chemical reactions. Among the BMNP, the CuO and NiO-based BMNPs are showing interesting properties because of their divalent, coloration and high reactivity. The Cu–Ni nanocatalyst was synthesized at various ratios by the micro-emulsion route (Ahmed et al. 2008). A surfactant-free and eco-friendly green methodology were adopted for the synthesis of Cu–Ni nanocatalyst (Nasrollahzadeh et al. 2019). Ni–Cu bimetallic nanoparticle was used for the catalytic reduction purpose (Bian et al.

2009). Cyanation of aryl halide was done effectively with the help of the prepared Cu–Ni nanocatalyst by the NaBH<sub>4</sub> reduction method (Mayakrishnan et al. 2020). A sol–gel method was adopted for the synthesis of Cu–Ni nanocatalyst (Quiroz et al. 2012). Similarly, the Cu–Ni nanocatalyst was used for various catalytic applications, such as reduction of nitrophenol and dyes (Ismail et al. 2018), selective hydrogenolysis of glycerol to 1,2-propanediol (Pudi et al. 2015), selective oxidation of benzaldehyde (Liu et al. 2019), reduction of *p*-nitrophenol (Vivek et al. 2020) and conversion of furfural into 2-methyl furan (Seemala et al. 2018). The application of nanocatalyst in the crosslinking of the natural polymer was not reported in the literature. This motivated the authors to do this research work.

Cyanuric chloride (CC) is a chlorine substituted triazine with antimicrobial activity. In chemistry, it is used as a crosslinking agent and is a temperature-dependent process. In the field of polymer chemistry, it is used as a crosslinking agent to increase the molecular weight of the polymer. Fujita et al. (2020) reported the CC cross-linked indoxyl-glucoside units for bio-molecular design. Cyanuric chloride crosslinked poly(divinylbenzene) was reported in the literature (Hao et al. 2020). The DSC study on CC crosslinked

✉ R. Anbarasan  
anbu\_may3@yahoo.co.in

<sup>1</sup> Department of Physics, Hajee Karutha Rowther Howdia College, Uthamapalayam, Tamil Nadu 625 533, India

<sup>2</sup> Department of Physics, Hindustan Institute of Technology and Science, Chennai, Tamil Nadu 603 103, India

<sup>3</sup> Department of Chemical Engineering, National Taiwan University, Taipei 10617, Taiwan

collagen was thoroughly studied by Chakarska et al. (2010). Cyanuric chloride was cross-linked with phenol sulphonic acid condensation product for the chromium-free tanning process. (Yu et al. 2020). The crosslinking of CC with PP fiber grafted styrene–divinylbenzene copolymers was done by Zhang and Li (2009). Similarly, The crosslinking of CC with polymeric materials, such as poly(ethylene oxide) for Li batteries (Tigelaar et al. 2006), hyper cross-linked polymer for CO<sub>2</sub> capture (Shao et al. 2018), elastomers for catalytic application (Fatona et al. 2020), amidoximated acrylic microfiber (Almulaity et al. 2018) and chitosan (Al Rasheed et al. 2020) was also carried out for certain end-use applications. The literature survey indicates that very few reports are available on the CC crosslinked biopolymers to increase the molecular weight of the same. In the present research work, the molecular weight of Lignin is increased via crosslinking reaction with CC at different feed ratios.

Lignin is a biopolymer with a polyphenolic structure. Extraction of organic soluble lignin is a commonly employed commercial process, but it yields only low molecular weight lignin. For certain end-use applications, the polymer should have high thermal and mechanical properties. This can be achieved through crosslinking of lignin using various crosslinking agents. Balakshin et al. (2020) reviewed the crosslinking of lignin. An increase in cell walls of lignin was achieved through ferulate crosslinking (Boutin et al. 2018). Lignin was technically crosslinked via esterification and free radical methods (Luo et al. 2018). Lignin hydrogel was prepared via crosslinking with PEG for medical applications (Larreneta et al. 2018). Enzymatically cross-linked lignin sulphonate was reported in the literature (Weiss et al. 2020). Lignin was grafted with dimethylaminoethyl methacrylate via the ATRP method (Lu et al. 2015). Lignin was crosslinked through phenolic reaction (Chen et al. 2020). Lignin was crosslinked with sulphated carbon for the selective removal of cationic dyes (Zhu et al. 2021). The main idea of the present research work is to increase the molecular weight of Lignin via surface crosslinking. Moreover, the study on crosslinking of Lignin with CC using BMNP as a catalyst is scarce in the documented literature.

Recently, the quality of the environment is highly diminished by the various activities of metal, chemical and dye industries. The degradation of individual pollutants is much easier than the mixture of pollutants because of the complex and intermediate product formation. To increase the efficiency of the degradation process, a nanocatalyst-based catalyst is being used. Recently, various techniques were followed for the degradation of Ar pollutants present in the effluent water (Yaswanth et al. 2019a, b). Sun et al. (2019) prepared a Cu–Ni nanocatalyst for the reduction of nitrophenol and dyes. Glainmer et al. (2021) reviewed the catalytic utilization of the nanocatalyst system for wastewater remediation. The Cu–Co nanocatalyst was used for the reduction

of nitroarenes and organic dyes (Gholinejad et al. 2020). Fe/Pd nanocatalyst-based catalyst was utilized for the reduction of Cr(VI) (Shi et al. 2019). Cu–Pd catalyst was used for the reduction of nitrate (Santos et al. 2020; Ullah et al. 2017). Reduction of Cr(VI) into Cr(III) was attempted in the presence of Cu–Ni as a nanocatalyst (Boreah et al. 2014). The reduction of Cr(VI) was examined using Cu/In oxysulphide nanocatalyst under dark condition (Chen and Kuo 2017). A conventional methodology was adopted for the synthesis of BMNP and characterized by various analytical methods. The novelty of the present study is the synthesis and utilization of CuO–NiO-based BMNP as a catalyst for the reduction of a mixture of effluents and indole derivative preparation in an effective manner. The BMNP is an effective catalyst and plays a vital role in the degradation of environmental pollutants.

## Experimental

All the required chemicals, such as CuSO<sub>4</sub>, NiSO<sub>4</sub>, CuI, Indole, benzaldehyde and iodobenzene were purchased from Showa Chemicals, India. Brilliant green (BG) dye, methanol, FeCl<sub>3</sub> and chloroethylamine were purchased from CDH chemicals, India. Potassium dichromate Cr(VI), *p*-nitrophenol (NTP), KOH and fluorescein (Flur) dye were procured from Merck, India. NaBH<sub>4</sub>, acetone, tetrahydrofuran (THF) and cyanuric chloride (CC) were purchased from Nice chemicals, India. Lignin (Lig) with the  $M_w = 8000$  g/mol and *N*-methyl pyrrolidone (NMP) were purchased from E. Merck, India.

A simple chemical reduction method was followed for the synthesis of CuO–NiO BMNP at different feed ratios, such as 4.0, 1.5, 0.66, 0.25 and 1.0. The synthesis procedure is mentioned below (Deka et al. 2021): The Cu to Ni ratio was kept as 1:1 for the preparation of BMNP. Equal concentrations of CuSO<sub>4</sub> and NiSO<sub>4</sub> were taken in a 250 mL round-bottomed flask (RBF) charged with 100 mL DDW under nitrogen purging. The chemical reduction was initiated by the addition of 10 g of hydrazinium hydroxide at room temperature under vigorous stirring condition. The chemical reduction of both Cu and Ni was confirmed by the change in color of the reaction medium. The content of the RBF was filtered and washed with acetone to remove the unreacted materials. The dried final mass of CuO–NiO BMNP was stored in a vial under a nitrogen atmosphere.

The molecular weight of Lignin before and after crosslinking with cyanuric chloride (CC) was analyzed by carrying out the gel permeation chromatography (GPC) analysis using Perkin Elmer Series 200 in THF solvent. The Brunauer–Emmett–Teller (BET) analysis was carried out and the active surface area of CuO–NiO BMNP was determined as 161 m<sup>2</sup>/g by nitrogen adsorption and

desorption method using BELSORP-max, Jp. Shimadzu 3600 NIR spectrophotometer, Jp was used to record the UV–visible spectra. The CuO–NiO BMNP formation was confirmed by HR-TEM using JEM 2100, Jp. The binding energy of the CuO–NiO BMNP was determined by XPS, Thermo Scientific, Theta Probe, UK. The functionalities present in the CuO–NiO BMNP were examined with the help of the FT-IR Shimadzu, Jp. The XRD was recorded on Bruker K 8600. The SEM with EDX was recorded on SEM, JSM 6300, JEOL model, US. The sample dispersed in DDW was used to record the fluorescence emission spectra on the Elico SL174, In.

The aqueous solution of a binary mixture of toxic pollutants was prepared by mixing 1 mL of  $10^{-5}$  M NTP solution with an equal concentration of Cr(VI) or Flur dye in DD water. Then it was mixed with 2 mg of CuO–NiO BMNP nano-catalyst and 15 mg of  $\text{NaBH}_4$  in a cuvette reactor. This reaction mixture was subjected to UV–visible spectral measurement at a regular interval of 1 min to monitor the pollutant reduction process. The catalytic reduction potential of CuO–NiO BMNP was understood by measuring the apparent rate constant ( $k_{\text{app}}$ ) using the recorded absorbance values (Chishti et al. 2021).

Indole and benzaldehyde were taken in a 2.2:1 ratio in 3 mL DDW. With this 3 mol% of CuO–NiO BMNP was added and stirred at room temperature for 1 h (Rafiee et al. 2009). At the end of the reaction, 3 mL of aliquot was pipetted out to carry out the UV–visible spectral measurement. The rate of reaction was computed using Eq. (1).

$$\text{Rate of reaction} = \frac{\text{Absorbance}}{\text{Volume} \times \text{time} \times \text{Molecular weight}} \times 1000 \quad (1)$$

An equal concentration of indole and iodobenzene was taken in a 10 mL round-bottomed flask (RBF). 5 mol% of CuI (0.025 mmol) and KOH (1 g) were added in a vigorous stirring condition under  $\text{N}_2$  atmosphere. The temperature of the reaction was maintained at 100 °C in NMP solvent. At the end of the reaction, 3 mL of aliquot was taken to carry out the UV–visible spectral measurement (Malavade et al. 2020).

1 g of BG dye was dispersed in NMP solvent (5 mL). Then, it was mixed with 0.50 g chloroethylamine and 0.10 g of  $\text{FeCl}_3$  (anhydrous) under vigorous stirring condition. The contents were heated at 65 °C for 2 h in the presence of 0.05 g of  $\text{K}_2\text{CO}_3$ . At the end of the reaction, the contents were filtered and freeze-dried (Yu et al. 2015). The dried product was dispersed in 3 mL DDW and subjected to UV–visible spectral analysis. A similar procedure was adopted for the preparation of BG dye derivative in the presence of 2 mg of CuO–NiO BMNP. The rate of reaction was determined using Eq. (1).

1.0 g of Lignin ( $M_w$  8000 g/mol) was dissolved in THF and treated with 1.0 g of CC at 0–5 °C for 1 h. Then the contents were precipitated by the addition of excess acetone. The dried mass was dissolved in THF (spectral grade) to perform the GPC measurement (Pardal et al. 2001). The crosslinking of Lig with CC was carried out at a different concentration of CuO–NiO BMNP using the above-mentioned experimental procedure. For all the samples, the  $M_n$ ,  $M_w$  and polydispersity (PD) values were calculated from the GPC traces.

## Results and discussion

### Characterizations

The UV–visible absorption spectrum of CuO–NiO BMNP is shown in Fig. 1a–e. It exhibited an absorbance peak at 394 nm associated with the Cu conjugated Ni nanoparticle. It was found that while increasing the Cu/Ni ratios, the absorbance value of the peak at 394 nm was gradually increased (Fig. 1a–e). Devi and Singh (2016) explained the UV–visible spectrum of Cu–Ni nanomaterial. The obtained result of our study is more similar to their report. This confirmed that both Cu and Ni can form BMNP easily. The direct bandgap of CuO–NiO BMNP was determined from Tauc's plot (Fig. 1f–j). The bandgap was found to be decreased from 5.45 to 4.85 eV with the increasing Cu to Ni ratio. The existence of chemical interaction between CuO and NiO in the BMNP was concluded by the decrease in bandgap value. The bandgap energy of Cu–Ni nanocatalyst was reported as 1.7 eV in the literature (Devi and Singh 2016). When compared with the literature report, the present research work produced higher bandgap energy due to the formation of CuO and NiO BMNP. The mixture of metaloxides and BMNP formation is further supported by XRD, HRTEM and XPS.

It is well known that both  $\text{Cu}^{2+}$  and  $\text{Ni}^{2+}$  are colored due to the  $d-d$  transition. Therefore, it exhibited the fluorescence property when the CuO–NiO BMNP was subjected to fluorescence emission spectrum (FES, excited at 400 nm) as shown in Fig. 2a–e. It showed an emission peak at 684 nm. One interesting point noted here is that the intensity at 684 nm was gradually increased while increasing the  $\text{Ni}^{2+}$  concentrations. This confirmed the fluorescence nature of CuO–NiO BMNP. Moreover, the prepared CuO–NiO BMNP is useful in photodynamic therapy, since both  $\text{Cu}^{2+}$  and  $\text{Ni}^{2+}$  are bio-compatible. Rahman et al. (2015) explained the FES of Cu–Au BMNP at 645 nm. When compared with the present work, the emission peak was red-shifted to 684 nm from its actual position for the CuO–NiO system. The redshift in the emission peak confirmed the formation of CuO–NiO BMNP, because the wavelength and emission intensity of

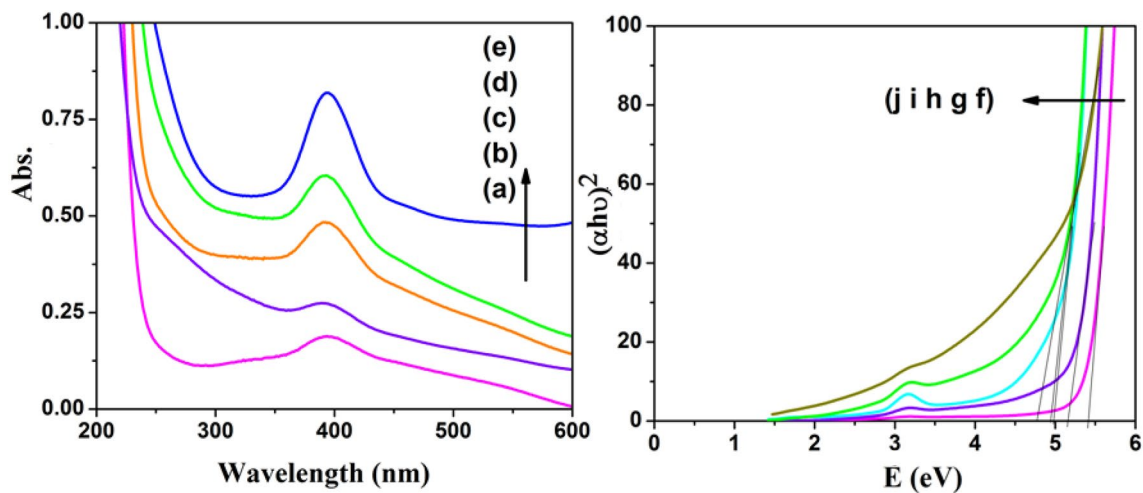


**Fig. 1** UV-visible absorption spectra and Tauc's plot of CuO–NiO BMNP synthesized at various Cu/Ni ratios of (a, f) 4.0, (b, g) 1.5, (c, h) 1.0, (d, i) 0.66, (e, j) 0.25, respectively

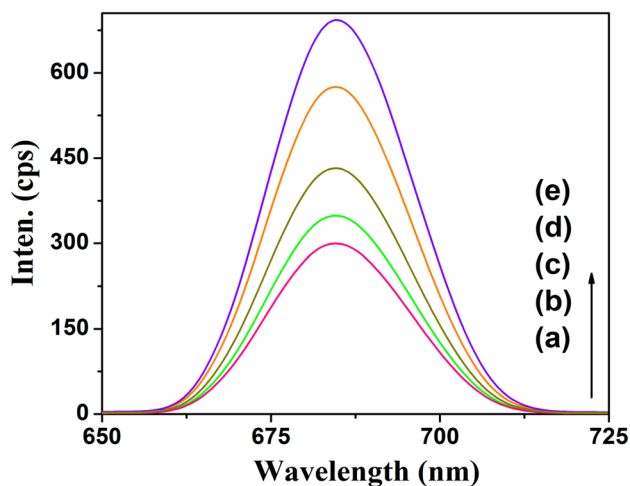


**Fig. 2** FES of Cu–Ni BMNP synthesized at various Cu/Ni ratios of (a) 4.0, (b) 1.5, (c) 1.0, (d) 0.66, (e) 0.25

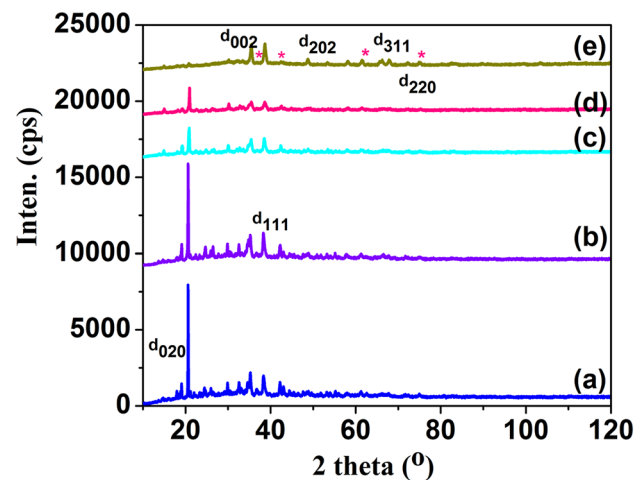


**Fig. 3** XRD of CuO–NiO BMNP synthesized at various Cu/Ni ratios of (a) 4.0, (b) 1.5, (c) 1.0, (d) 0.66, (e) 0.25

the peaks are greater than that of the individual metal ion. Moreover, the emission intensity of the peak depends on the concentration of the BMNP. The crystal structure of BMNP was further confirmed by XRD.

The FT-IR spectrum of synthesized CuO–NiO BMNP at different Cu to Ni ratios is given in Fig. S1a–e. The spectrum showed the Cu–O stretching ( $477\text{ cm}^{-1}$ ) and Ni–O stretching ( $585\text{ cm}^{-1}$ ) (Devi and Singh 2016). While increasing the  $\text{Ni}^{2+}$  concentrations, the peak at  $477\text{ cm}^{-1}$  associated with the CuO stretching became sharp. The FT-IR spectrum confirmed that both Cu and Ni are present in their mono-oxide form. Since the FT-IR spectrum of the BMNP exhibited peaks at  $477$  and  $585\text{ cm}^{-1}$  corresponding to the metal-oxides stretching which led to the conclusion of the formation of metaloxides during the preparation of BMNP.

Hence, the FT-IR spectrum simply provided information about the nature of functional groups available in the system. The crystal structure of the mixture of metaloxides and BMNP was also confirmed by XRD.

The crystalline structure of CuO–NiO BMNP was confirmed by XRD (Fig. 3a–e). At the lower Cu to Ni ratio, the diffractogram exhibited peaks corresponding to Cu, Ni, CuO and NiO NPs, whereas the diffractogram showed only peaks corresponding to CuO and NiO for the prepared BMNP at a higher Cu/Ni ratio. Peaks at  $20.65^\circ$  ( $d_{020}$ ),  $32.5^\circ$  ( $d_{002}$ ),  $35.5^\circ$  ( $d_{222}$ ),  $38.4^\circ$  ( $d_{111}$ ),  $42.8^\circ$  ( $d_{002}$ ),  $72.3^\circ$  ( $d_{220}$ ) are corresponding to Cu NP (Singh et al. 2016). The  $d$  value was determined as  $4.85\text{ \AA}$  for the assigned peak at  $20.65^\circ$ . Peaks corresponding to CuO NP are  $61.6^\circ$  ( $d_{113}$ ),  $48.8^\circ$  ( $d_{202}$ ),  $58.1^\circ$  ( $d_{202}$ ),  $66.0^\circ$  and  $67.8^\circ$  ( $d_{331}$ ). This is in accordance with

the JCPDS File No. 5-0661. The crystallite size was calculated as 32 nm by the Sherrer formula. Peaks at  $24.7^\circ$ ,  $25.9^\circ$ ,  $75.09^\circ$  ( $d_{311}$ ),  $53.4^\circ$  ( $d_{200}$ ),  $75.1^\circ$  ( $d_{311}$ ) are corresponding to NiO NP (JCPDS, File No. 04-0835). The crystal structure of NiO was found to be FCC. It was found that the intensity of the peak at  $20.65^\circ$  ( $d_{020}$ ) corresponding to CuO was slowly decreased and finally disappeared with the increasing concentration of  $\text{Ni}^{2+}$ . Here the Cu/Ni ratio was noted as 0.25. This study declared that the added Ni compound controlled the crystal growth of Cu during the BMNP formation, because while increasing the concentration of  $\text{Ni}^{2+}$ , the intensity of the peak at  $20.65^\circ$  slowly decreased and finally disappeared. This proved that the prepared final product contains a mixture of components (i.e.) BMNP formation and a mixture of metal oxides. The crystallite size was also confirmed by HR-TEM.

The outermost electronic configuration of CuO–NiO BMNP was confirmed by XPS analysis (Fig. 4). The binding energy confirmed that the elements of Ni and Cu are present in the form of oxides, such as NiO and CuO. Furthermore, it was confirmed by the HR-TEM technique. The O1s appeared at 530.1 eV. The  $\text{Ni}2p_{3/2}$  and  $\text{Ni}2p_{1/2}$  appeared at 855.8 and 874.9 eV, respectively. The  $\text{Cu}2p_{3/2}$  and  $\text{Cu}2p_{1/2}$  appeared at 930.4 and 952.3 eV, respectively (Zhang et al. 2015). The XPS confirmed that there was a formation of a mixture of CuO–NiO and BMNP. Moreover, the appearance of O1s peak confirmed the formation of BMNP through the oxides of Cu and Ni (i.e.) a mixture of CuO and NiO.

### SEM with EDX study

Figure 5a indicates the SEM image of CuO–NiO BMNP. The image showed distorted spherical particles with a fluorescent surface. Again this confirmed the  $d$ – $d$  transition present in the metal ions and metaloxides. Thus the SEM image

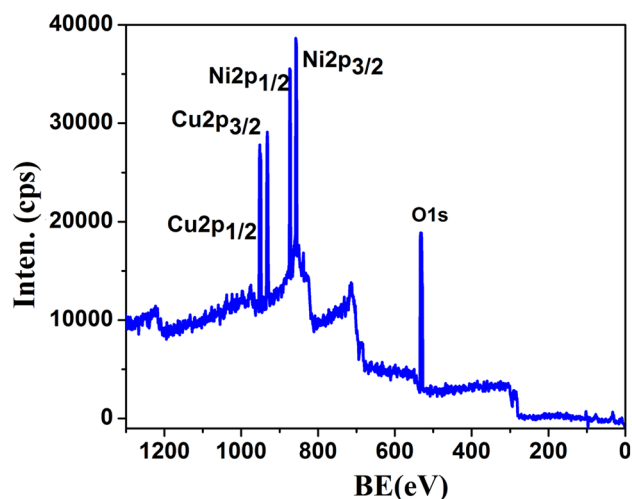


Fig. 4 XPS of Cu–Ni BMNP synthesized at Cu/Ni = 1.0

supported the FES of a mixture of metal oxides and BMNP. Moreover, the particles are in an agglomerated state. Moganavally et al. (2014) thoroughly studied the SEM image of CuO–NiO BMNP. Our report is coinciding with their report. Figure 5b represents the EDX spectrum of CuO–NiO BMNP. The spectrum showed O (0.53 keV), Ni (748 keV), Cu (800 keV) peaks with the atomic weight % of 9.9, 45.8 and 44.3, respectively. This confirmed the 1:1 ratio of Cu and Ni. The EDX report also confirmed the formation of CuO and NiO BMNP.

The CuO–NiO BMNP formation was confirmed by HR-TEM analysis. Figure 6a, b indicates the mixture of metaloxides and BMNP formation. One of the metal oxides is spherical in shape, whereas the other one appears with a distorted spherical shape (Zhang et al. 2015). The size of the spherical particles was found to be  $\sim 20$  nm, whereas

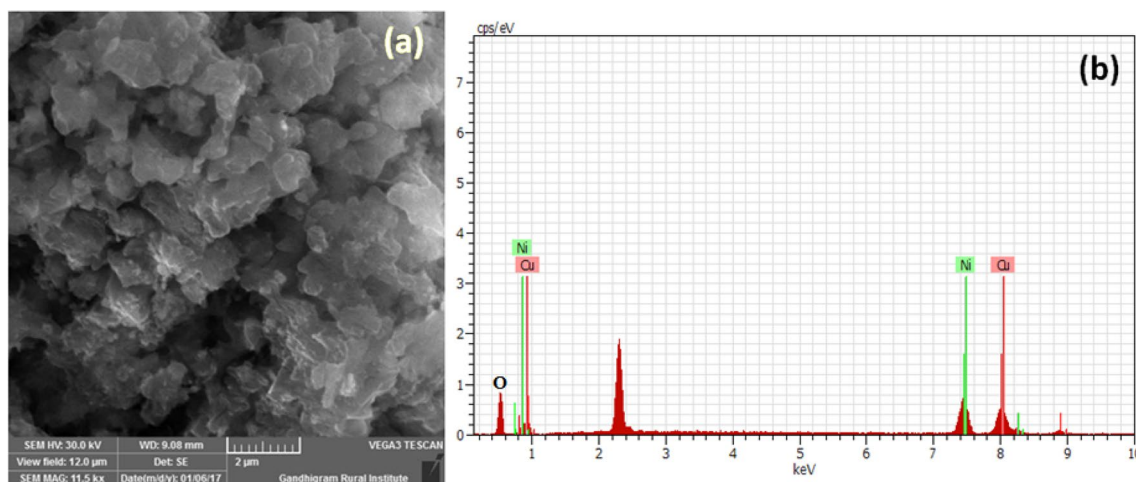
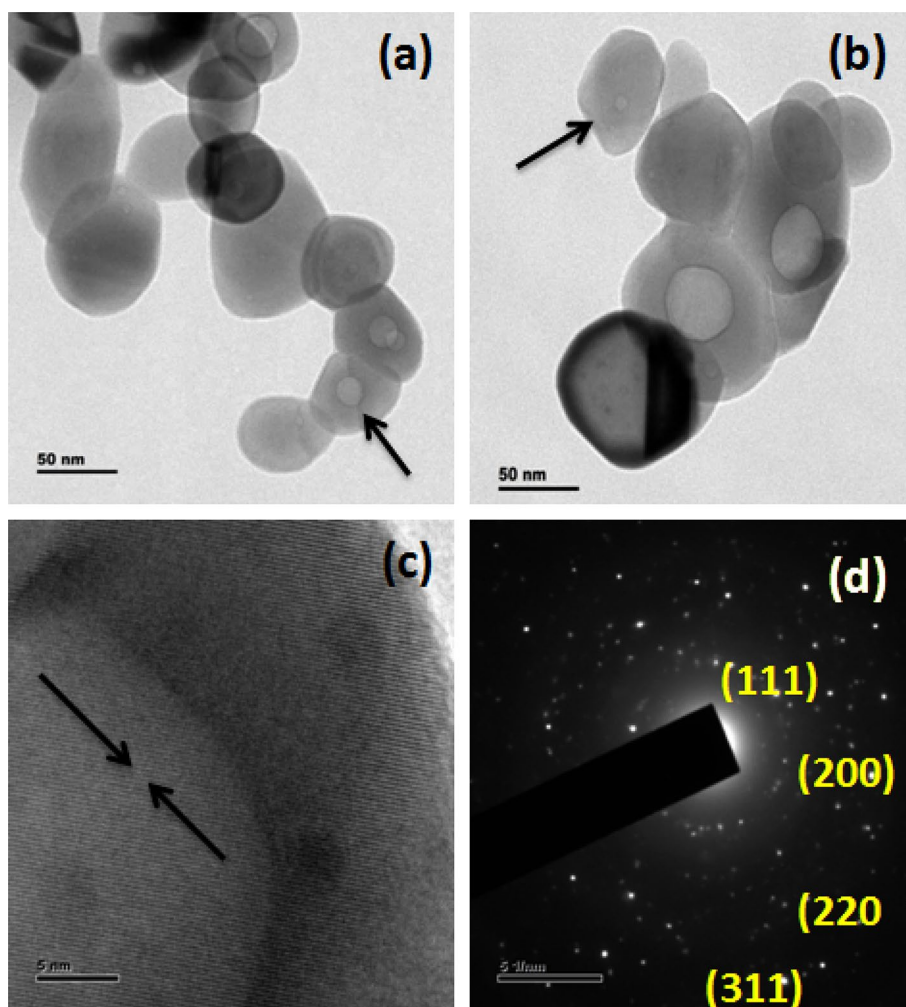


Fig. 5 a SEM image and b EDX spectrum of CuO–NiO BMNP synthesized at the Cu/Ni ratio of 1.0

**Fig. 6** **a, b** HR-TEM image, **c** perfect grain structure and **d** SAED pattern of CuO–NiO BMNP



distorted spherical particles were found to be 50–80 nm in length. Thus the result of HR-TEM was in accordance with XRD. Figure 6c represents the perfect grain structure of BMNP (indicated by an arrow mark). The SAED pattern of CuO–NiO BMNP is shown in Fig. 6d with  $d_{(111)}$ ,  $d_{(200)}$  and  $d_{(311)}$  peaks of oxides of Cu and Ni. The distance between the two crystal planes is determined as 0.12 nm. These crystal planes are corresponding to mono oxides of Cu and Ni. Moreover, here one can see the core–shell-like structure in HR-TEM, and the mixture of CuO and NiO was concluded from XRD. The SAED also confirmed the crystalline nature of the mixture of oxides and BMNP. Hence, the HR-TEM supported the XRD and XPS data.

### Catalytic reduction study

A UV–visible spectrophotometer is an ideal tool to follow the catalytic reduction kinetics of various environmental pollutants particularly the Cr(VI) (Amala Jeya Ranchani et al. 2017). The catalytic reduction of binary pollutant mixture systems, such as Cr(VI)—NTP, NTP—Flur dye, and

Cr(VI)—Flur dye was performed using CuO–NiO BMNP as a catalyst. For the reduction study, an equal concentration of binary pollutant was taken individually along with 15 mg of  $\text{NaBH}_4$  and 1 mg of CuO–NiO BMNP catalyst in a 3 mL quartz cuvette. The reactants were shaken well before recording the UV–visible spectrum. The UV–visible spectrum was captured at every 1 min time interval. The efficiency of the prepared catalyst was assessed by measuring the apparent rate constant ( $k_{\text{app}}$ ) value.

The catalytic performance of CuO–NiO BMNP nanocatalyst on the reduction of Cr(VI) and NTP binary pollutant mixture was investigated by capturing UV–visible spectra at every 1 min interval (Fig. 7a–o). All the spectra showed only one absorbance peak at 390 nm which confirmed the complex formation between the Cr(VI) and NTP. The efficient reduction of Cr(VI) and NTP pollutant mixture was concluded by the decrement in the intensity of the absorbance peak at 390 nm in the presence of CuO–NiO BMNP catalyst.

The  $k_{\text{app}}$  value was evaluated as  $0.0153 \times 10^{-2} \text{ s}^{-1}$  (Table 1) from a graph of  $\ln(A/A_0)$  vs time as illustrated in Fig. 7p to assess the pollutant reduction efficiency of CuO–NiO

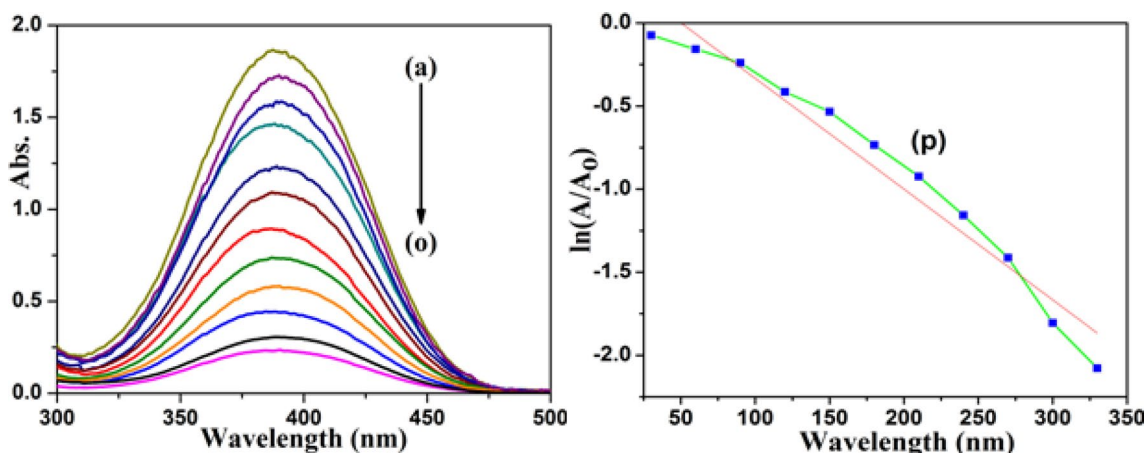


**Fig. 7** a–o UV–visible spectrum of binary mixture of Cr(VI)–NTP system and the plot of  $\ln(A/A_0)$  against time (p)

**Table 1**  $k_{app}$  value for different systems

System	$k_{app} (s^{-1}) \times 10^{-2}$			
	NTP	Cr(VI)	Flur	Complex
NTP + Flur	0.0502	–	0.0116	–
Cr(VI) + Flur	–	0.0217	0.0212	–
Cr(VI) + NTP	–	–	–	0.0153

BMNP catalyst. The Mg-AC (Amala Jeya Ranchani et al. 2019) mediated catalytic reduction of Cr(VI) + NTP mixture yielded the  $k_{app}$  value of  $3.41 \times 10^{-2} s^{-1}$ . When compared with the literature value, the present work yielded a lower  $k_{app}$  value due to the agglomerated nature of CuO–NiO BMNP and the formation of a strong complex between Cr(VI) and NTP. The complex formation between Cr(VI) and NTP was previously discussed in our publication (Amala Jeya Ranchani et al. 2021).

The reduction of a binary mixture of Cr(VI)–Flur dye was studied in the presence of CuO–NiO BMNP nano-catalyst by capturing the UV–visible spectra at every 1 min interval (Fig. 8a–q). The absorbance peaks associated with Cr(VI) and Flur dye were noticed at 375 nm and 490 nm, respectively. The intensity of the absorbance peaks was notably decreased with the reaction time. The gradual reduction in absorbance authentically proved the reduction of a binary mixture of Cr(VI) and Flur dye into nontoxic products. The  $k_{app}$  value for the prepared catalyst was determined by measuring slope values from the plot of  $\ln(A/A_0)$  vs time as illustrated in Fig. 8r, s. The  $k_{app}$  values were estimated as  $0.0217 \times 10^{-2} s^{-1}$  for Cr(VI) reduction and  $0.0212 \times 10^{-2} s^{-1}$  (Table 1) for Flur dye reduction, respectively. When compared with the AC-Mg system, (Amala Jeya Ranchani et al. 2019), the present work yielded a lower  $k_{app}$  value (Table 2).

When compared with the literature reports, the present system produced lower  $k_{app}$  values towards the catalytic

reduction of NTP, Cr(VI) and Flur dye. In the literature, the  $k_{app}$  value was determined for the individual component, but in the present research work, it is determined for the mixture of components particularly for the bicomponent or tricomponent systems. When the NTP is present in its mixture form, there is a chance for the formation of a stable complex with the other pollutants present in the system. The complex formation will reduce the reduction behavior of NTP or Cr(VI) or Flur dye. It is well known that both Cu and Ni are effective catalysts. However, they produced a lower  $k_{app}$  value due to the stable complex formation of the pollutants. In overall comparison, one can say that the present system yielded excellent results when the pollutants are in their mixture form.

The reduction of a binary mixture of NTP–Flur dye was examined using the CuO–NiO BMNP as a catalyst. The reduction study was monitored by recording the UV–visible spectra as shown in Fig. S2(a–p). The presence of two absorbance peaks at 395 nm and 490 nm are attributed to NTP and Flur dye, respectively. The absorbance corresponding to these peaks was decreased with the reduction time. It proved the conversion of a binary mixture of NTP and Flur dye into eco-friendly products (i.e.) aminophenol and a reduced form of Flur dye. The efficiency of the prepared catalyst on the reduction of NTP–Flur dye was determined by plotting a graph of  $\ln(A/A_0)$  vs time as shown in Fig. S2(r, q). The  $k_{app}$  values were estimated as  $0.0502 \times 10^{-2} s^{-1}$  (Table 1) for NTP and  $0.0116 \times 10^{-2} s^{-1}$  for Flur dye. The reduction of NTP was 85% in 10 min and the reduction of Flur dye was 99% in 16 min for the NTP and Flur dye mixture. The obtained  $k_{app}$  values are too low as compared with the literature values of  $3.06 \times 10^{-2}$  for NTP and  $2.30 \times 10^{-2} s^{-1}$  for Flur dye reduction (Amala Jeya Ranchani et al. 2019).

The catalytic activity of CuO–NiO BMNP was tested towards the preparation of indole derivatives. As mentioned in Scheme 1, the prepared sample was analyzed by

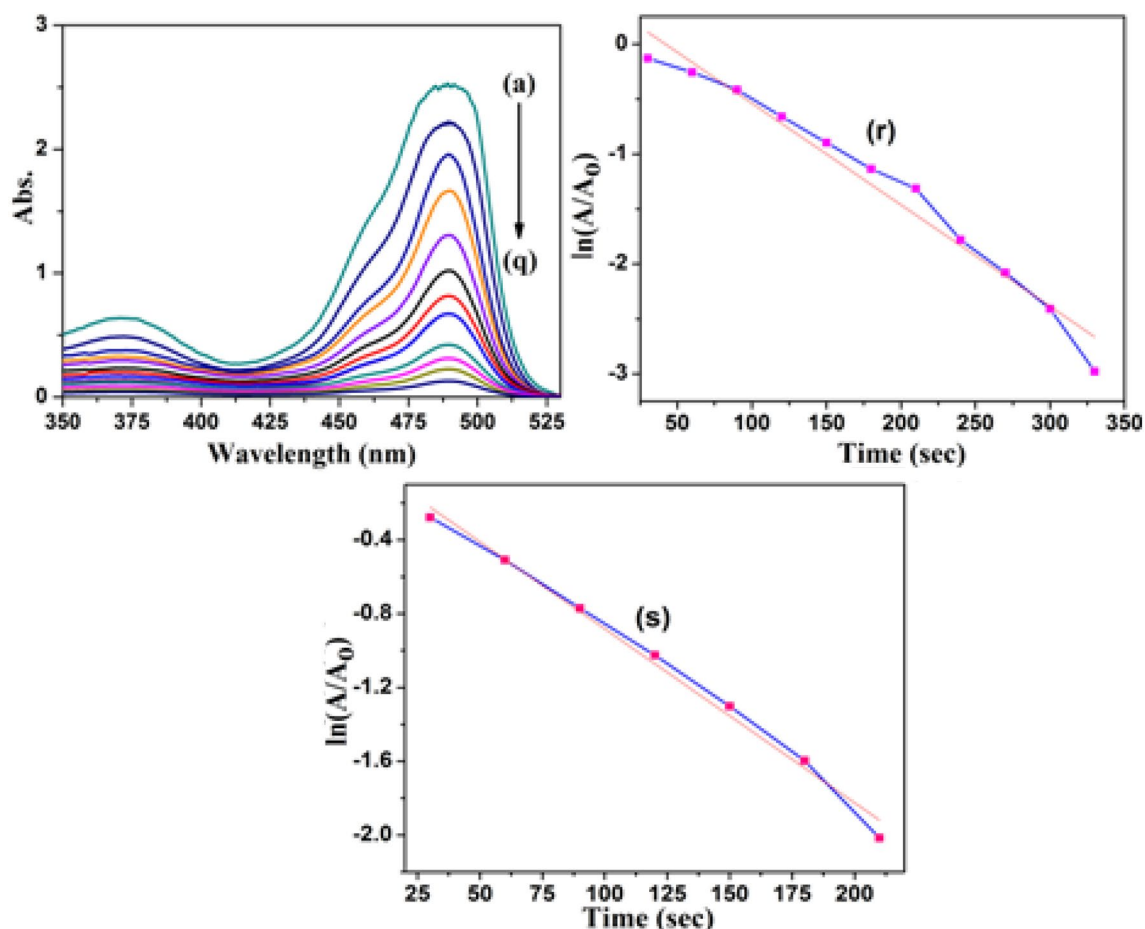


**Fig. 8** a–q UV–visible spectrum of binary mixture of Cr(VI)—Flur dye, (r) plot of  $\ln(A/A_0)$  against time for Cr(VI) and (s) plot of  $\ln(A/A_0)$  against time for Flur dye

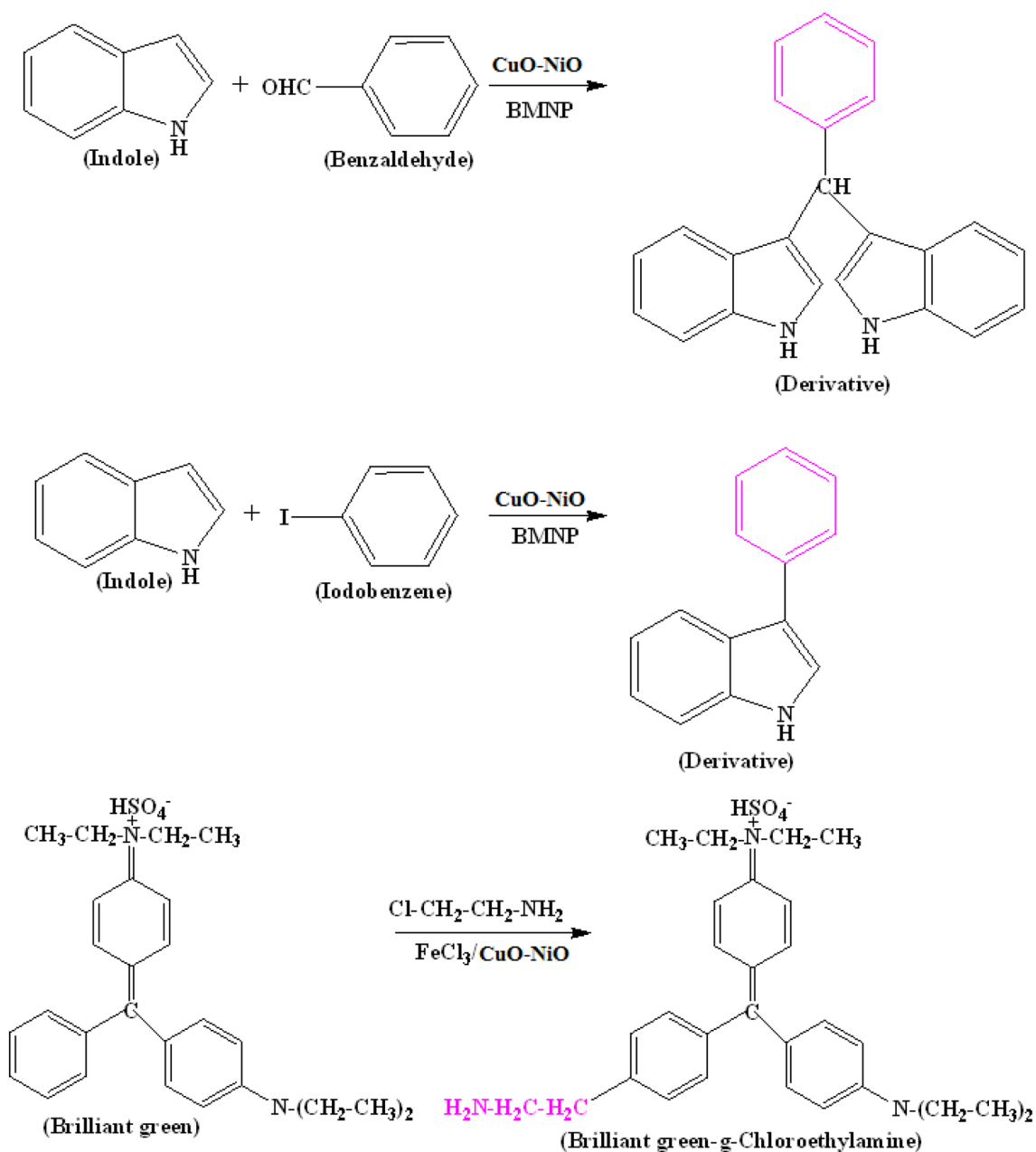
**Table 2**  $k_{app}$  value of various pollutants

System	Author, year	$k_{app}$ ( $s^{-1}$ )	Catalyst
NTP	Patharawadee et al. (2018)	$1 \times 10^{-2}$	Ni
	Das et al. (2015)	$7 \times 10^{-3}$	Au
	Dash et al. (2014)	$4.1 \times 10^{-3}$	Au
	Amala Jeya Ranchani et al. (2020)	$4.26 \times 10^{-2}$	Cu
	Present	$0.0502 \times 10^{-2}$	BMNP
Cr(VI)	Amala Jeya Ranchani et al. (2020)	$6.11 \times 10^{-2}$	Cu
	Amala Jeya Ranchani et al. (2019)	$0.128 \times 10^{-2}$	Ca
	Present	$0.0217 \times 10^{-2}$	BMNP
Flur	Amala Jeya Ranchani et al. (2020)	$4.84 \times 10^{-2}$	Cu
	Amala Jeya Ranchani et al. (2019)	$5.82 \times 10^{-2}$	Ca
	Present	$0.0116 \times 10^{-2}$	BMNP

a UV–visible spectrophotometer. The UV–visible spectrum of pure indole is portrayed in Fig. 9A(a). It exhibits two absorbance peaks below 300 nm due to the  $\pi$  to  $\pi^*$  transition and  $n$  to  $\pi^*$  transitions (i.e.) a transition of  $\pi$  electrons to the excited  $\pi^*$  level and the transition

of non-bonding electrons to the excited  $\pi^*$  level. The direct treatment of indole with benzaldehyde leads to indole derivative [Fig. 9A(b)] with the absorbance value of 0.0581. The rate of reaction was computed as  $4.3709 \times 10^{-6}$  mol/lit/s (Table 3). The same indole derivative was prepared in the presence of CuO–NiO BMNP and the UV–visible spectrum is given in Fig. 9A(c) with the absorbance value of 0.1224. The rate of reaction was calculated as  $10.4671 \times 10^{-6}$  mol/lit/s (Table 3). The absorbance value is directly proportional to the concentration of the indole derivative. Hence, the increase in absorbance confirmed the catalytic activity of CuO–NiO BMNP towards the preparation of indole. In comparison, the rate of reaction was 2.5 times higher in the presence of CuO–NiO BMNP catalyst. This declared that the CuO–NiO BMNP could catalyze the indole derivative during the reaction process. It is very difficult to compare the catalytic efficiency of CuO–NiO BMNP with the available literature because of the non-availability of the rate of reaction. The present system proved the





**Scheme 1** Synthesis of indole and BG dye derivatives

catalytic activity of BMNP towards the indole derivative preparation.

The catalytic activity of CuO–NiO BMNP was further confirmed by the preparation of the benzene derivative of indole. This derivative was prepared both in the presence and absence of a catalyst. Figure 9B(a) indicates the UV–visible spectrum of neat indole with one broad absorbance peak at 277 nm associating with the  $\pi$  to  $\pi^*$  transition. The derivative prepared in the absence of catalyst doesn't show any absorbance peak [Fig. 9B(b)]. It means that there is no product formation in the absence of a

catalyst. Figure 9B(c) confirmed the product formation in the presence of CuO–NiO BMNP. The spectrum showed two major peaks with one shoulder peak. The peaks at 263 and 331 nm are associated with the  $\pi$  to  $\pi^*$  transition and the benzene derivative of indole, respectively. Apart from these, the shoulder peak at 399 nm was appeared due to the two phenyl ring substituted indole. The appearance of multiple peaks confirmed the catalytic activity of CuO–NiO BMNP towards the indole derivative preparation. The rate of reaction was determined as  $1.65 \times 10^{-5}$  mol/lit/s from the UV–visible absorbance value (Table 3). The higher rate of

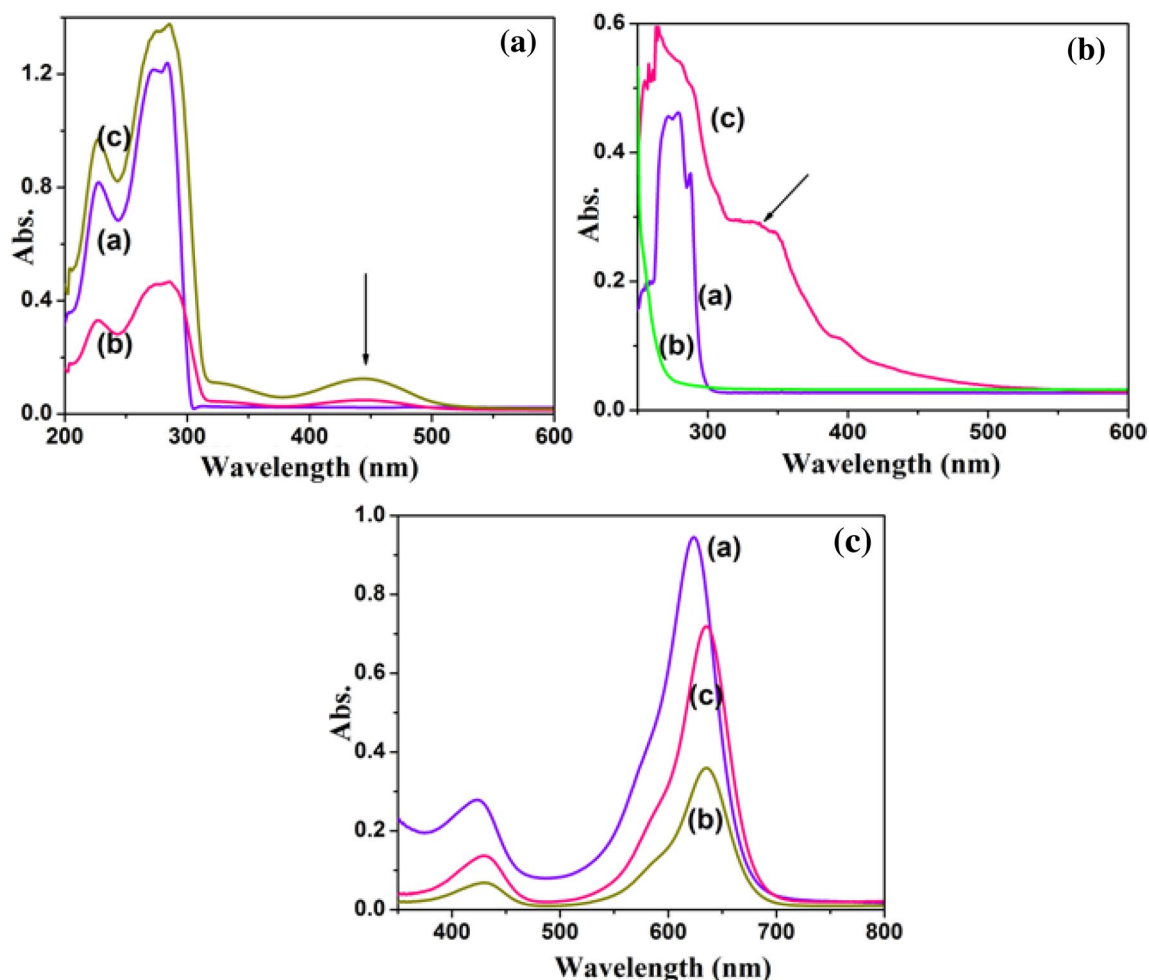


**Fig. 9** **a** UV-visible spectrum (a) neat indole, indole-benzaldehyde derivative prepared in the absence (b) and (c) presence of CuO-NiO BMNP. **b** UV-visible spectrum of (a) neat indole, indole-iodobenzene derivative prepared in the absence (b) and (c) presence of Cu-Ni

BMNP. **c** UV-visible spectrum of (a) neat BG dye, BG dye-chloroethylamine derivative prepared in the (b) absence and (c) presence of CuO-NiO BMNP catalyst

reaction confirmed the catalytic activity of CuO-NiO BMNP towards the indole derivative preparation. There is no rate of reaction available in the literature report for the prepared

indole derivative. However, this proved that one can prepare the indole derivative in the presence of BMNP catalyst with a good % yield.

**Table 3** Determination of rate of reaction for different derivative preparation

System	$\lambda_{\max}$ (nm)	Rate (mol/lit/s)
Indole	284	–
Indole + benzaldehyde	445	$4.3709 \times 10^{-6}$
Indole + benzaldehyde + CuO-NiO BMNP	445	$10.4671 \times 10^{-6}$
Indole + iodobenzene	–	–
Indole + iodobenzene + CuO-NiO BMNP	340	$1.65 \times 10^{-5}$
BG dye	622	–
BG dye + CEA	635	$1.2040 \times 10^{-5}$
BG dye + CEA + CuO-NiO BMNP	635	$2.4759 \times 10^{-5}$

The catalytic activity of CuO-NiO BMNP was further supported by the preparation of brilliant green (BG) dye derivative. The neat BG dye showed two absorbance peaks at 424 and 624 nm [Fig. 9C(a)]. After the Friedel-Crafts alkylation reaction in the absence of catalyst, it shows two peaks but with redshift [427 and 636 nm, Fig. 9C(b)]. The absorbance value was determined as 0.3606 from the UV-visible spectrum, and the rate of reaction was calculated as  $1.2040 \times 10^{-5}$  mol/lit/s (Table 3) using the absorbance value. For the sake of comparison, the CuO-NiO BMNP catalyzed BG dye derivative was prepared by Friedel-Crafts reaction. The UV-visible spectrum (433 and 636 nm) is given in Fig. 9C(c) with an absorbance value of 0.7191. The rate of reaction was calculated as  $2.4759 \times 10^{-5}$  mol/lit/s (Table 3). The increase in rate of

reaction confirmed the catalytic activity of CuO–NiO BMNP towards the BG dye derivative preparation. There is no standard literature report available for the rate of reaction. The present investigation proved that the structure of BG dye can be modified while preparing its derivative in the presence of a BMNP catalyst.

The surface catalytic effect of CuO–NiO BMNP was confirmed by the increasing molecular weight ( $M_w$ ) of Lignin. The  $M_w$  of neat Lignin was 8000 g/mol (Fig. S3a). When it was treated with cyanuric chloride (CC), the  $M_w$  of Lignin was increased to 8288 g/mol (Fig. S3b). The conjugations of Lignin with CC were carried out under ideal experimental conditions by varying the concentration of CuO–NiO BMNP, such as 2, 4, 6, 8 and 10 mg, and their corresponding GPC images are given in Fig. S3c–g. The data pertaining to this analysis is given in Table 4. The reaction process is described in Scheme S1. It was found that the  $M_w$  of Lignin was increased while increasing concentration of CuO–NiO BMNP. This can be explained as follows: the second chlorine atom of CC cannot be replaced by the –OH group of Lignin at 0–5 °C. Hence, the role of CC in increasing the  $M_w$  of Lignin is voided. It means that the added CuO–NiO BMNP played a vital in the Lignin molecular weight increment. Table 4 shows the GPC data for different systems. The  $M_w$  of Lignin was slowly increased with the increasing the concentration of CuO–NiO BMNP. This is explained as follows: the CuO–NiO BMNP is acting as a crosslinking center through polyol methodology during the treatment. This type of result was reported in the literature (Jeyapriya et al. 2015). The plot of log (weight of CuO–NiO BMNP) vs log  $M_w$  was drawn to comprehend the order of reaction (Fig. S3h). The plot was found to be a straight line with a slope value of 0.479. The  $M_w$  of Lignin was increased in the order of 0.479 with the increasing concentration of CuO–NiO BMNP. This further proved the active participation of CuO–NiO BMNP towards the increase in molecular weight of Lignin via surface catalytic effect. The surface area of the prepared catalyst is given in the experimental

part. There is no standard literature available to compare with this result.

### Catalytic reaction mechanism

It is well known that the CuO–NiO catalyst is a porous material with an active surface area of 161 m<sup>2</sup>/g. During the catalytic reduction of hazardous pollutant, such as NTP or Cr(VI), the pollutant was first adsorbed on the surface of the catalyst and then that was temporarily accommodated in the porous structure of the catalyst. Moreover, the reducing agent such as NaBH<sub>4</sub> is also adsorbed on the surface which leads to the reduction reaction (Amala Jeya Ranchani et al. 2021). Once the reaction is over, the reduced product was pushed out automatically by temperature which led to further reduction. In the case of indole derivative preparation, the reactants are also adsorbed on the surface of the catalyst. On the surface itself, the reaction occurred and the products are formed. Due to the change in surface energy, the formed products are diffused into the reaction medium. In the case of Lignin, the catalyst interacted with the –OH of Lignin and acted as a crosslinking center. In such a way more Lignin chains are adsorbed on the surface of the catalyst through the –OH group of Lignin. A similar type of effect was noted by Jeyapriya et al (2015) while using Ag nanoparticles as a crosslinking center. Now the Lignin chains are acting as an end-capping agent or stabilizing agent. In such a way, the molecular weight of Lignin was increased.

### Conclusions

The CuO–NiO BMNP was successfully synthesized by varying the Cu/Ni ratios. The absorbance at 394 nm gradually increased for the prepared CuO–NiO BMNP while increasing the concentration of Ni<sup>2+</sup>. The direct bandgap value of BMNP was decreased with the increase of Ni<sup>2+</sup> concentration. The emission intensity at 684 nm was increased while increasing the Ni<sup>2+</sup> concentration. The M–O stretching was noted at 477 cm<sup>−1</sup> for CuO and 595 cm<sup>−1</sup> for NiO in the FT-IR spectrum. The XRD results declared that the NiO controlled the crystal growth of CuO nanoparticles. The XPS showed the O1s, Ni2p and Cu2p peaks corresponding to the CuO–NiO BMNP. The SEM image of CuO–NiO BMNP showed distorted spherical morphology with a fluorescent surface. The EDX data confirmed the 1:1 ratio of Cu and Ni present in the prepared CuO–NiO BMNP. The HR-TEM image showed the defected grain structure of CuO–NiO BMNP. The catalytic reduction study confirmed the complex formation between Cr(VI) and NTP. The CuO–NiO BMNP mediated indole derivative and BG dye derivative exhibited higher rate constant values. The molecular weight of Lignin cross-linked CC was increased

**Table 4** GPC data

System	Weight of CuO–NiO BMNP (mg)	$M_w$ (g/mol)	$M_n$	PD
Lignin	–	8000	7272	1.1
Lignin + CC	–	8228	6329	1.3
Lignin + CC	2	12,515	8343	1.5
Lignin + CC	4	13,970	8217	1.7
Lignin + CC	6	16,739	12,876	1.3
Lignin + CC	8	20,137	16,780	1.2
Lignin + CC	10	23,678	13,154	1.8

with the increasing concentration of CuO–NiO BMNP, since it acted as a crosslinking center. The order of reaction was estimated as 0.479 for this process. This study successfully proved the catalytic potential of CuO–NiO BMNP.

**Supplementary Information** The online version contains supplementary material available at <https://doi.org/10.1007/s13204-021-02326-0>.

**Acknowledgements** I would like to thank Dr.N.Sundararajan, Associate Professor, Department of English, KCET, Madurai for his valuable help during this manuscript preparation work.

**Funding** There is no funding for this research work.

## Declarations

**Conflict of interest** On behalf of all authors, the corresponding author states that there is no conflict of interest.

## References

- Ahmed J, Ramanachary KV, Lofland SE, Ganguli AK (2008) Bimetallic Cu–Ni nanoparticles of varying composition (CuNi<sub>3</sub>, CuNi, Cu<sub>3</sub>Ni). *Coll Surf A Physicochem Eng Asp* 331:206–212. <https://doi.org/10.1016/j.colsurfa.2008.08.007>
- Almulaity YQ, Aqlan FM, Alayafi M (2018)  $\alpha$ -Amylase immobilization of amidoximated acrylic microfibers activated by cyanuric chloride. *R Soc Open Sci* 5:172164. <https://doi.org/10.1098/rsos.172164>
- Al Rasheed HH, Dahlous KA, Sholkamy EN, Faham AE (2020) Chitosan-*S*-triazinyl bis(2-aminomethylpyridine) and chitosan-*S*-triazinyl-bis(8-oxyquinoline) derivatives: new reagents for Ag nanoparticle preparation and their effect of antimicrobial evolution. *J Chem* 2020:1–8. <https://doi.org/10.1155/2020/9590120>
- Amala Jeya Ranchani A, Anitha Devi A, Parthasarathy V, Anbarasan R (2017) Catalytic activity of Ni complexed aminoclay towards the reduction of Cr(VI), *p*-nitrophenol and fluorescein dye. *Appl Nanosci* 7:655–666. <https://doi.org/10.1007/s13204-017-0609-4>
- Amala Jeya Ranchani A, Parthasarathy V, Anbarasan R (2019) Removal of hazardous pollutants from waste water. Catalytic applications of Mg nanoparticle functionalized aminoclay. *J Mol Liq* 296:112005. <https://doi.org/10.1016/j.molliq.2019.112005>
- Amala Jeya Ranchani A, Parthasarathy V, Anbarasan R (2020) Structural modification of aminoclay for catalytic applications. *Chem Eng Commun* 207:871–886. <https://doi.org/10.1080/00986445.2019.1630394>
- Amala Jeya Ranchani A, Parthasarathy V, Mahalakshmi S, Anbarasan R (2021) Facile synthesis of Fe nanospheres anchored aminoclay and its catalytic reduction of hazardous pollutants and oxidation activity. *J Dispers Sci Technol* 42(11):1640–1650. <https://doi.org/10.1080/01932691.2020.1776129>
- Balakshin M, Capanena EA, Zhu X, Rosenau T, Rojas OJ (2020) Spruce milled lignin: linear, branched or crosslinked? *Green Chem* 22:3985–4001. <https://doi.org/10.1039/d0gc00926a>
- Bian J, Xiao M, Wang SJ, Liu YX, Meng YZ (2009) Graphite oxide as a novel host material of catalytically active Cu–Ni bimetallic nanoparticle. *Catal Commun* 10:1529–1533. <https://doi.org/10.1016/j.catcom.2009.04.009>
- Boreah BJ, Saikia H, Bharati P (2014) Reductive conversion of Cr(VI) to Cr(III) over bimetallic nanoparticle at room temperature. *New J Chem* 38:2748–2751. <https://doi.org/10.1039/C4NJ00150H>
- Boutin ALC, Lapiere C, Alvarado C, Barron C, Devaux, Guillon F (2018) Ferulate and lignin crosslinks increases in cell walls of wheat grain outer layers during late development. *Plant Sci* 276:199–207. <https://doi.org/10.1016/j.plantsci.2018.08.022>
- Chakarska L, Todinova S, Ilakieva K (2010) Investigation on chemical crosslinked collagen phosphoric acid hydrolysates with cyanuric chloride by differential scanning calorimetry. *J Therm Anal Calorim* 102:1–7. <https://doi.org/10.1007/s10973-010-0905-7>
- Chen X, Kuo DH (2017) Nanoflower bimetal CuInOS catalyst for the reduction of Cr(VI) in the dark. *ACS Sustain Chem Eng* 5:4133–4143. <https://doi.org/10.1021/acssuschemeng.7b00107>
- Chen S, Wang G, Sui W, Parvez AM, Si C (2020) Synthesis of lignin functionalized phenolic nanospheres supported Ag nanoparticles with excellent dispersion stability and catalytic performance. *Green Chem* 22:2879–2888. <https://doi.org/10.1039/C9GC04311J>
- Chishti AN, Guo F, Aftab A, Ma Z, Liu Y, Chen M, Gautam J, Chen C, Ni L, Diao G (2021) Synthesis of silver doped Fe<sub>3</sub>O<sub>4</sub>/C nanoparticles and its catalytic activities for the degradation and reduction of methylene blue and 4-nitrophenol. *Appl Surf Sci* 546:147070. <https://doi.org/10.1016/j.apsusc.2021.149070>
- Das S, Braja GB, Ranadhir B (2015) *Saraca indica* bark extract mediated green synthesis of polyshaped gold nanoparticles and its application in catalytic reduction. *Appl Nanosci* 5:867–873. <https://doi.org/10.1007/s13204-014-0384-4>
- Dash SS, Rakhi M, Arun KS, Braja GB, Biplab KP (2014) *Saraca indica* bark extract mediated green synthesis of polyshaped gold nanoparticles and its application in catalytic reduction. *Appl Nanosci* 4:485–490. <https://doi.org/10.1007/s13204-013-0223-z>
- Deka JR, Saikia D, Lu NF, Chen KT, Kao HM, Yans KC (2021) Space confined synthesis of highly dispersed bimetallic CoCu nanoparticles as effective catalyst for ammonia borane dehydrogenation of 4-nitrophenol reduction. *Appl Surf Sci* 538:148091. <https://doi.org/10.1016/j.apsusc.2020.148091>
- Devi HS, Singh TD (2016) Cu–Zn and Cu–Ni bimetallic nanoparticles using ascorbic acid and its role in photo-degradation of methyl orange. *Asian J Chem* 28:2255–2260. <https://doi.org/10.14233/ajchem.2016.19544>
- Fatona A, Osamudiamen A, Mirabal JM, Brook MA (2020) Rapid catalyst free cross linking of silicones using triazines. *J Polym Sci* 1:1–11. <https://doi.org/10.1021/pol.20200289>
- Fujita H, Zhang Y, Wu Z, Lindsey (2020) Chromogenic agents built around a multifunctional double triazine framework for enzymatically triggered cross linking under physiological conditions. *New J Chem* 44:3856–3867. <https://doi.org/10.1039/C9NJ06187H>
- Gholinejad M, Naghbari Z, Sansaou JM (2020) Co/Cu bimetallic ZIF as new heterogeneous catalyst for reduction of nitroarenes and dyes. *Appl Organomet Chem* 34:e5522. <https://doi.org/10.1002/aoc.5522>
- Glainmer K, Lu MC, Huang YH (2021) Synthesis and catalytic utilization of bimetallic systems for waste water remediation. *Chemosphere* 262:128371. <https://doi.org/10.1016/j.chemosphere.2020.128371>
- Hao A, Wang S, Huang J (2020) Filling the pores of the post cross linked polymers with different rigid cross linking bridges. *Chem Select* 5:7941–7946. <https://doi.org/10.1002/slct.202001861>
- Ismail M, Khan MI, Khan SB, Khan MA, Akhtar K (2018) Green synthesis of plant supported Cu–As and Cu–Ni bimetallic nanoparticles in the reduction of nitrophenols and organic dyes for water treatment. *J Mol Liq* 260:78–91. <https://doi.org/10.1016/j.molliq.2018.03058>
- Jeyapriya M, Meenarathi B, Anbarasan R (2015) Synthesis and characterization of nano Ag end capped L-cysteine bridged diblock

- copolymer. *Chin J Polym Sci* 33:1404–1420. <https://doi.org/10.1007/s10118-015-1688-x>
- Larreneta E, Imizcoz M, Toh JX, Irvin NJ, Ripolin A, Perminova A, Donelleg RF (2018) Synthesis and characterization of lignin hydrogels for potential applications as drug eluting antimicrobial coatings for medical materials. *ACS Sustain Chem Eng* 6:9037–9046. <https://doi.org/10.1021/acssuschemeng.8601371>
- Liu L, Zhou X, Liu L, Jiang S, Tai X (2019) Heterogeneous bimetallic Cu–Ni nanopowder supported catalysts in the selective oxidation of benzyl alcohol to benzaldehyde. *Catalysis* 9:1–18. <https://doi.org/10.3390/catal.9060538>
- Lu X, Yin H, Zhang Z, Diao B, Li J (2015) Functionalization of lignin through ATRP grafting of poly(2-dimethylaminoethylmethacrylate) for gene delivery. *Colloids Surf B Biointerfaces* 125:230–237. <https://doi.org/10.1016/j.colsurb.2014.11.018>
- Luo S, Cao J, McDonald AG (2018) Cross linking of technical lignin via esterification and thermally initiated free radical reaction. *Ind Crop Prod* 121:169–179. <https://doi.org/10.1016/j.indcrop.2018.05.007>
- Malavade V, Patil M, Patil M (2020) Scope, kinetics and mechanism of on water Cu catalysis in the C–N cross coupling reaction of indole derivative. *Eur J Chem* 5:561–569. <https://doi.org/10.1002/ejoc.2019.01542>
- Mayakrishnan G, Elappan V, Kim IS, Chung IM (2020) Sea island like morphology of Cu–Ni bimetallic nanoparticle uniformly anchored on single layer grapheme oxide as a highly efficient and noble metal free catalyst for cyanation of aryl halides. *Sci Rep* 10:677–692. <https://doi.org/10.1038/s41598-020-57483-2>
- Moganavally P, Suresh R, Deepa M (2014) Synthesis and characterization of bimetallic Cu–Ni nanoparticles. *J Appl Chem* 7:34–36
- Nasrollahzadeh M, Sajjadi M, Komber H, Sajjadi SM (2019) *In situ* green synthesis of Cu–Ni bimetallic nanoparticles supported on reduced grapheme oxide as an effective and recyclable catalyst for the synthesis of *N*-benzyl-*N*-aryl-5-amino-1*H*-tetrazoles. *Appl Organomet Chem* E4938:1–14. <https://doi.org/10.1002/aoc.4938>
- Pardal AC, Ramos SS, Sandos L, Almeida P (2001) Synthesis and fixation of aminocyanines to microcrystalline cellulose using cyanuric chloride as a cross linking agent. *Color Technol* 117:43–48
- Patharawadee B, Surangkana M, Sittipong A (2018) Highly catalytic activity of nickel nanoparticles generated in poly(methylmethacrylate)@poly(2-hydroxyethylmethacrylate) (PMMA@PHEMA) core–shell micelles for the reduction of 4-nitrophenol (4-NP). *Appl Nanosci* 8:475–488. <https://doi.org/10.1007/s13204-018-0669-0>
- Pudi SM, Biswas P, Kumar S, Sankar B (2015) Selective hydrogenolysis of glycerol to 1,2-propanediol over bimetallic Cu–Ni catalysts supported on  $\gamma$ -Al<sub>2</sub>O<sub>3</sub>. *J Braz Chem Soc* 26:1551–1564. <https://doi.org/10.5935/0103-5053.20150123>
- Quiroz L, Obregon DV, Cerda G (2012) Synthesis and characterization of alloy and bimetallic nanoparticle of Cu–Ni prepared by sol-gel method. *Mater Res Soc Symp Proc* 1479:9–15. <https://doi.org/10.1557/opl.2012.1590>
- Rafiee E, Zolfagharifar Z, Hoshghavi J, Eavani S (2009) Facile condensation of indole with benzaldehyde over Keggin type heteropoly compounds: an initial effect toward catalyst design. *Appl Catal A Gen* 365:287–291. <https://doi.org/10.1016/j.apcata.2009.06.030>
- Rahman L, Shah A, Qureshi R, Khan SB, Zia MA (2015) Spectroscopic analysis of Au–Cu alloy nanoparticles of various compositions synthesized by a chemical reduction method. *Adv Mater Sci Eng* 2015:638629. <https://doi.org/10.1155/2015/638629>
- Santos G, Restiro J, Orge A, Soares P (2020) Nitrate catalytic reduction over bimetallic catalysis: catalyst optimization. *J Carbon Res* 6:78–90. <https://doi.org/10.3390/c6040078>
- Seemala B, Cai CM, Kumar R, Chrostopher P (2018) Effects of Cu–Ni bimetallic catalyst composition and support on activity, selectivity and stability for conversion to 2-methyl furan. *Sustain Chem Eng* 6:2152–2161. <https://doi.org/10.1021/acssuschemeng.7603572>
- Shao L, Sang Y, Huang J, Liu YN (2018) Triazine based hyper cross linked polymers with inorganic–organic hybrid frame work derived porous carbons for CO<sub>2</sub> capture. *Chem Eng J* 353:1–14. <https://doi.org/10.1016/j.cej.2018.07.108>
- Shi D, Ouyang Z, Zhao Y, Shi X (2019) Catalytic reduction of hexavalent chromium using Ir/Pd bimetallic nanoparticle assembled filter paper. *Nanomaterials* 9:1183. <https://doi.org/10.3390/nano9081183>
- Singh PK, Kumar P, Hussain M, Das AK, Nayak GC (2016) Synthesis and characterization of CuO nanoparticles using strong base electrolyte through electro-chemical discharge process. *Bull Mater Sci* 39:469–478. <https://doi.org/10.1007/s12034-016-1159-1>
- Sun H, Zelekew OA, Lu Q, Lin J (2019) A noble bimetal oxysulfide CuVOs catalyst for highly efficient catalytic reduction of 4-nitrophenol and organic dyes. *RSC Adv* 9:31828–31839. <https://doi.org/10.1039/C9r905172d>
- Tigelar DM, Meador B, Kinder JD, Bennet WR (2006) New APTES cross linked polymers from PEO and cyanuric chloride for Li batteries. *Macromolecules* 39:120–127. <https://doi.org/10.1021/ma051657d>
- Ullah I, Khan K, Sohail M, Ullah A, Shaheen S (2017) Synthesis, structural characterization and catalytic application of citrate stabilized monometallic and bimetallic Pd@Cu nanoparticles microbial anti activities. *Int J Nanomed* 12:8735–8747. <https://doi.org/10.2147/IJNS145085>
- Vivek S, Preethi S, Kumar V, Suresh Babu K (2020) Oxidation studies on mono (Cu, Ni) and bimetallic (Cu–Ni) nanoparticles and its impact on catalytic activity. *J Alloy Compd* 81b:152608. <https://doi.org/10.1016/j.jallcom.2019.152608>
- Weiss R, Ghitti E, Hasinger MS, Nyahongo GS (2020) Lignin based pesticide delivery system. *ACS Omega* 5:4322–4329. <https://doi.org/10.1021/acsomega.9b04275>
- Yaswanth KP, Ganapathi A, Janakarajan R, Kamal KK (2019a) Redox synergistic Mn–Al–Fe and Cu–Al–Fe ternary metal oxide nano adsorbents for arsenic remediation with environmentally stable As(0) formation. *J Hazard Mater* 364:519–530. <https://doi.org/10.1016/j.jhazmat.2018.10.069>
- Yaswanth KP, Nidhi T, Shambunath J, Dibyendu B, Janakarajan R, Kamal KK (2019b) Arsenic surface complexation behavior in aqueous systems onto Al substituted Ni Co, Mn, and Cu based ferrite nano adsorbents. *J Hazard Mater* 361:383–393. <https://doi.org/10.1016/j.jhazmat.2018.07.056>
- Yaswanth KP, Amit KY, Iram M, Alekha T, Janakarajan R, Kamal KK (2021) Insights of arsenic (III/V) adsorption and electrosorption mechanism onto multi synergistic (redox-photoelectrochemical-ROS) Aluminium substituted Copper Ferrite impregnated rGO. *Chemosphere* 267:129246. <https://doi.org/10.1016/j.chemosphere.2020.129246>
- Yu H, Cao Y, Kang G, Kuang W, Zhou M (2015) Enhancing the anti-fouling properties of PSF-ultrafiltration membranes by the grafting of PEG derivatives via surface amidation reaction. *J Appl Polym Sci* 132:41870. <https://doi.org/10.1021/app.41870>
- Yu L, Qians X, Cui L, Chen B, Wang X, Wu X (2020) Preparation of a syntan containing active chlorine groups for chrome-free tanned leather. *J Clean Prod* 270:122351. <https://doi.org/10.1016/j.jclea.2020.122351>
- Zhang Y, Li D (2009) PP fibre grafted styrene-divinylbenzene copolymers post cross linked with cyanuric chloride. *Iran Polym J* 18:617–622
- Zhang S, Zhang Z, Zhang X, Zhang J (2015) Novel bimetallic Cu/Ni core-shell nanoparticles and nitrogen doped GQDs composites applied in glucose in vitro detection. *PLoS ONE* 14:e02200305. <https://doi.org/10.1371/journal.pone.0220005>

Zhu S, Xu J, Kuang Y, Cheng Z, Chen K (2021) Lignin derived sulfonated porous carbon from cornstalk for efficient and selective removal of cationic dyes. *Indus Crop Prod* 159:113071. <https://doi.org/10.1016/j.indcrop.2020.113071>

**Publisher's Note** Springer Nature remains neutral with regard to jurisdictional claims in published maps and institutional affiliations.